

## Research Article

# CCII and FPGA Realization: A Multistable Modified Fourth-Order Autonomous Chua's Chaotic System with Coexisting Multiple Attractors

Fei Yu <sup>1</sup>, Hui Shen <sup>1</sup>, Li Liu <sup>1</sup>, Zinan Zhang <sup>1</sup>, Yuanyuan Huang <sup>1</sup>, Binyong He <sup>1</sup>, Shuo Cai <sup>1</sup>, Yun Song <sup>1</sup>, Bo Yin <sup>1</sup>, Sichun Du <sup>2</sup>, and Quan Xu <sup>3</sup>

<sup>1</sup>School of Computer and Communication Engineering, Changsha University of Science and Technology, Changsha 410114, China

<sup>2</sup>College of Computer Science and Electronic Engineering, Hunan University, Changsha 410082, China

<sup>3</sup>School of Information Science and Engineering, Changzhou University, Changzhou 213164, China

Correspondence should be addressed to Fei Yu; [yufeiyf@csust.edu.cn](mailto:yufeiyf@csust.edu.cn) and Yuanyuan Huang; [snailhy@126.com](mailto:snailhy@126.com)

Received 25 December 2019; Accepted 12 February 2020; Published 21 March 2020

Guest Editor: Viet-Thanh Pham

Copyright © 2020 Fei Yu et al. This is an open access article distributed under the Creative Commons Attribution License, which permits unrestricted use, distribution, and reproduction in any medium, provided the original work is properly cited.

In this paper, a multistable modified fourth-order autonomous Chua's chaotic system is investigated. In addition to the dynamic characteristics of the third-order Chua's chaotic system itself, what interests us is that this modified fourth-order autonomous Chua's chaotic system has five different types of coexisting attractors: double-scroll, single band chaotic attractor, period-4 limit cycle, period-2 limit cycle, and period-1 limit cycle. Then, an inductorless modified fourth-order autonomous Chua's chaotic circuit is proposed. The active elements as well as the synthetic inductor employed in this circuit are designed using second-generation current conveyors (CCIIs). The reason for using CCIIs is that they have high conversion rate and operation speed, which enable the circuit to work at a higher frequency range. The Multisim simulations confirm the theoretical estimates of the performance of the proposed circuit. Finally, using RK-4 numerical algorithm of VHDL 32-bit IQ-Math floating-point number format, the inductorless modified fourth-order autonomous Chua's chaotic system is implemented on FPGA for the development of embedded engineering applications based on chaos. The system is simulated and synthesized on Virtex-6 FPGA chip. The maximum operating frequency of modified Chua's chaotic oscillator based on FPGA is 180.180 MHz. This study demonstrates that the hardware-based multistable modified fourth-order autonomous Chua's chaotic system is a very good source of entropy and can be applied to various embedded systems based on chaos, including secure communication, cryptography, and random number generator.

## 1. Introduction

Nonlinear phenomena widely exist in natural science, engineering technology, and social science. Since 1960, the research and application of nonlinear systems have been more and more extensive. Many problems in complex networks [1–7], memristor [8–11], electronic circuits [12–15], image processing [16–21], economics [22], and other fields can be attributed to the study of nonlinear systems. Chaos is a special state of motion in a nonlinear system, which is a random-like behavior generated by a deterministic system and is extremely sensitive to initial values and highly dependent on them [23–28]. Entropy is

usually used to describe the complexity of chaotic systems. Therefore, it is of great significance to study the entropy of nonlinear systems [29–31].

With the rapid development of computer technology, the accompanying information security issues have attracted more and more attention and become a hot issue [32–42]. Chaos is widely used in cryptosystems, random numbers, and secure communications [43–49], and it has become a hot topic in nonlinear circuits and systems. In the realization of chaotic circuits, researchers have proposed many new methods to design different types of chaotic circuits [50–55]. Among them, Chua's chaotic circuit [56–58] has attracted wide attention because of its simple structure, bifurcation,

and chaotic complex dynamic characteristics. There are many research contents and achievements on this circuit, such as Chua's dual circuit [59], transformed Chua's circuit [60], multiscroll Chua's circuit [61], and hyperchaotic Chua's circuit [62, 63].

Multistability is a critical property of nonlinear dynamical systems, where a variety of behaviors such as coexisting attractors can appear for the same parameters, but different initial conditions. The flexibility in the system's performance can be archived without changing parameters [64, 65]. This has become a very popular research topic and some important research results have been achieved recently [11, 66–69]. In [66], a 4D memristor-based Colpitts system was proposed by employing an ideal memristor to substitute the exponential nonlinear term of original 3D Colpitts oscillator model, from which the initials-dependent extreme multistability was exhibited by phase portraits and local basins of attraction. In [67], an ideal voltage-controlled memristor emulator-based canonical Chua's circuit was investigated. With the voltage-current model, the initial condition-dependent extreme multistability was explored through analyzing the stability distribution of line equilibrium point and then the coexisting infinitely many attractors were numerically uncovered in such a memristive circuit by the attraction basin and phase portraits. In [69], a 5D multistable four-wing memristive hyperchaotic system (FWMHS) with linear equilibrium points was proposed by introducing a flux-controlled memristor model with absolute value function. A secure communication scheme based on the proposed 5D multistable FWMHS with disturbance inputs was also designed. To our best knowledge, fourth-order autonomous Chua's chaotic systems with multistability are rare in literature. Therefore, it is of great significance to study a fourth-order Chua's chaotic system with multistability.

In recent years, there exist several studies related to fourth-order autonomous Chua's chaotic circuits [70–73]. The design of a new fourth-order autonomous nonlinear electric circuit using two active elements, one linear negative conductance, and one nonlinear resistor has been proposed by Koliopoulos et al. to show rich dynamic behavior of Chua's circuit [71]. In the performed study by Liu et al., the design of fourth-order Chua's circuit has been proposed with a piecewise-linear nonlinearity and with a smooth cubic nonlinearity which could produce different kinds of attractors [72]. Wang et al. designed a fourth-order Chua's circuit using a capacitor, a resistance, and a controlled-source constituted by stair functions in the third-order Chua's circuit which could generate multidirectional multiscroll (MDMS) chaotic attractors [73]. However, the passive inductors are used in the circuits proposed in [70–73]. In fact, the parameters of passive inductor are not only difficult to control accurately in the actual Chua's circuit, but also very easy to be affected by frequency, environment, and other factors. Generally speaking, the internal resistance of the inductor will affect the oscillating circuit, and the larger the value of the inductor, the greater the internal resistance of the inductor, and the greater the impact on the circuit. In order to minimize the influence

of the internal resistance of the inductor on the circuit, the actual inductor can be replaced by the active inductor in the experiment. The active inductor can be equivalent to the ideal inductor without internal resistance consumption [74, 75].

Meanwhile, these modified Chua's circuits generally use ordinary voltage-mode operational amplifiers as active devices. Because the gain-bandwidth product of voltage-mode operational amplifiers is limited (usually several megahertz), it is necessary to balance the gain and bandwidth in the design of circuits. That is to say, in order to get a large circuit gain, the operating frequency of the circuit can only be reduced [76–79]. And the current-mode devices have good frequency gain characteristics. The bandwidth of these kind of devices is almost independent of gain, so there is no need to weigh the gain and bandwidth in the designed circuit, which can improve the working frequency of the circuit [80]. In recent years, the current-mode devices to realize Chua's circuit have gradually become a new research direction. In [81], active simulated inductor and piecewise nonlinear resistor in the circuit were all realized by second-generation current conveyors (CCII), so that the circuit was more stable and can work in higher frequency than does the usual Chua's circuit. The circuit also had the advantages in that the current waves and the corresponding phase diagrams could be tested easily. Jothimurugan et al. [82] reported an improved implementation of an inductorless third-order autonomous canonical Chua's circuit. The active elements as well as the synthetic inductor employed in this circuit were designed using current feedback operational amplifiers (CFOAs). The implementation of inductorless makes the experimental construction of Chua's circuit simple and compact.

Many analog implementations of chaotic systems in electronic circuits have been reported in recent decades, such as the well-known breadboard with discrete components [10, 13, 27, 28] and CMOS technology for integrated circuit (IC) design [12, 23, 24]. However, breadboard is not easy to carry, maintain, and store data, and IC design has a long cycle and high cost [83–87]. Meanwhile, in some chaotic information systems, digital implementation may be necessary, for example, in embedded chaos-based application areas and many other chaotic digital information systems. Digital chaotic generators have been implemented by varied structures such as Digital Signal Processor (DSP) [88, 89] and Field Programmable Gate Array (FPGA) [90–94]. In order to calculate complex mathematical operations, the DSP chips are optimized operations sequentially. Constant-time autonomous chaotic systems are characterized by at least three differential equations and at least three outputs. Therefore, it takes a long time for systems based on DSP to calculate the output signal values in turn. On the other hand, the FPGA chip can run in parallel and has a relatively flexible architecture. Therefore, the design and test cycle cost of the FPGA chip is extremely low. Moreover, because of its reprogrammability, high speed, and large capacity, the implementation of FPGA is of great significance in the fields of information security, encryption, cryptography, communication, and other applications [95, 96].

In recent years, the design of chaotic system based on FPGA has been extensively studied. In [90], by the help of fourth-order of RK4 method, Sundarapandian-Pehlivan chaotic system was proposed in VHDL 32-bit IEEE 754-1985 floating-point number standard on Virtex-6 FPGA chip. In [91], autonomous Lu-Chen chaotic system was implemented on Virtex-6 FPGA chip using Heun numerical algorithm in VHDL 32-bit IQ-Math fixed-point number format. In [92], with the method of Artificial Neural Networks, the design of Pehlivan-Uyaroglu chaotic system was implemented in VHDL IEEE 754 single precision floating-point number format on Virtex-6 FPGA chip. A 3D nonequilibrium chaotic system using RK4 numerical algorithm with IEEE 754-1985 floating-point number standard on Virtex-6 FPGA chip was designed in [93]. In [94], the implementation of multibutterfly chaotic system in FPGA by applying the Xilinx (Vivado) system generator was proposed.

The objective of this study is twofold. First, based on a multistable modified fourth-order autonomous Chua's chaotic circuit introduced in [70], an improved implementation of an inductorless modified fourth-order autonomous Chua's chaotic circuit is proposed. The active elements as well as the synthetic inductor employed in this circuit are designed using CCIs. The reason for employing CCIs is that, compared with circuits designed with voltage operational amplifiers, CCIs have better characteristics such as high conversion rate and high working speed, so that the circuit can work in higher frequency ranges. Second, the RK-4 method in a hardware description language (VHDL) is used to model the modified fourth-order autonomous Chua's chaotic system, and the model is tested comprehensively on Xilinx Virtex-6 FPGA chip. The phase portraits of the output result of the system based on FPGA are given. The design results of the modified Chua's chaotic oscillator based on FPGA are compared with those of computer, which verifies the correctness of the design based on digital circuit.

The structure of this paper is as follows: a multistable modified fourth-order autonomous Chua's chaotic system is investigated and the dynamic characteristics are discussed in Section 2. An inductorless modified fourth-order autonomous Chua's chaotic circuit is constructed by using CCI in Section 3. The Multisim simulation results of the inductorless modified Chua's chaotic circuit are also given. In Section 4, the FPGA-based model of the modified fourth-order autonomous Chua's chaotic system is introduced and simulation results of FPGA-based model are presented. Finally, conclusions are outlined in Section 5.

## 2. Multistable Modified Fourth-Order Autonomous Chua's Chaotic System

**2.1. Modified Fourth-Order Autonomous Chua's Chaotic Circuit.** By adding a linear resistor and a linear capacitor to the classical Chua's chaotic circuit, a modified fourth-order autonomous Chua's chaotic circuit is introduced in [70], as shown in Figure 1. According to Kirchhoff's law, the dynamics of this circuit is governed by the following equations:

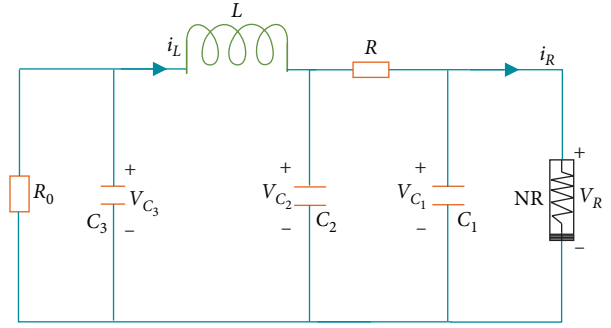


FIGURE 1: Modified fourth-order autonomous Chua's chaotic circuit.

$$\begin{cases} C_1 \frac{dV_{C_1}}{dt} = \frac{1}{R} (V_{C_2} - V_{C_1}) - f(V_{C_1}), \\ C_2 \frac{dV_{C_2}}{dt} = \frac{1}{R} (V_{C_1} - V_{C_2}) + i_L, \\ L \frac{di_L}{dt} = V_{C_3} - V_{C_2}, \\ C_3 \frac{dV_{C_3}}{dt} = -i_L - \frac{1}{R_0} V_{C_3}, \end{cases} \quad (1)$$

where  $V_{C_1}$ ,  $V_{C_2}$ ,  $V_{C_3}$ , and  $i_L$  are state variables which denote the voltage across  $C_1$ , the voltage across  $C_2$ , the voltage across  $C_3$ , and current through  $L$ , respectively. According to the principle of Chua's diode in classical Chua's chaotic circuit, the characteristic curve of Chua's diode NR in (1) can be graphically represented as in Figure 2 and is given by

$$f(V_{C_1}) = G_b V_{C_1} + \frac{1}{2} (G_a - G_b) \times (|V_{C_1} + E_a| - |V_{C_1} - E_a|), \quad (2)$$

where  $G_a$  and  $G_b$  are the slopes of the outer and inner regions, respectively, and  $\pm E_a$  denote the breakpoints.

### 2.2. Multistable Modified Fourth-Order Autonomous Chua's Chaotic System

**2.2.1. System Generation and Dynamics Analysis.** When  $x = V_{C_1}/E_a$ ,  $y = V_{C_2}/E_a$ ,  $z = i_L R/E_a$ ,  $w = V_{C_3}/E_a$ ,  $\alpha = C_2/C_1$ ,  $\beta = C_2 R^2/L$ ,  $\gamma_1 = R/R_0$ ,  $\gamma_2 = C_2/C_3$ , equation (1) can be expressed as follows:

$$\begin{cases} \dot{x} = \alpha [y - x - f(x)], \\ \dot{y} = x - y + z, \\ \dot{z} = -\beta (y - w), \\ \dot{w} = -\gamma_2 (z + \gamma_1 w). \end{cases} \quad (3)$$

When the parameters are selected as  $C_1 = 10$  nF,  $C_2 = 100$  nF,  $L = 17.64$  mH,  $R = 1.68$  k $\Omega$ ,  $C_3 = 2$   $\mu$ F,  $E_a = 1$ ,  $G_a = -1.28$  ms,  $G_b = -0.69$  ms, and  $R_0 = 60$   $\Omega$ , we can get  $\alpha = 10$ ,  $\beta = 16$ ,  $\gamma_1 = 28$ , and  $\gamma_2 = 0.05$ . A double-scroll chaotic

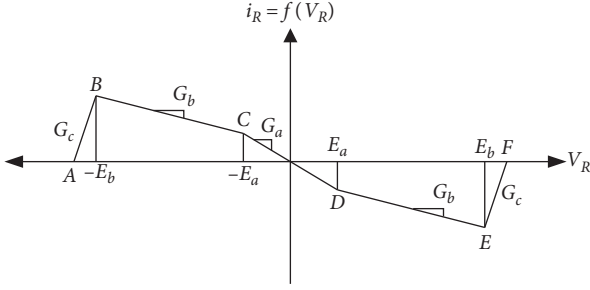


FIGURE 2: Five-segment piecewise linear  $V - I$  characteristic of the nonlinear resistor.

attractor is generated by MATLAB simulation under the initial condition  $[0, 0.1, 0, 0]$ , as shown in Figure 3. As can be seen from Figure 3, when the parameters of the system satisfy certain conditions, a self-excited oscillation attractor called double-scroll, like Chua's circuit, will also be generated. Chaotic orbits are currents circling around strange attractors [59]. The nonperiodicity of chaotic oscillation can be clearly seen from the time-domain waveforms, as shown in Figure 4.

The dynamic system described by differential equation (3) is symmetric with respect to origin and corresponds to the characteristics of Chua's diode NR. If the characteristics of Chua's diode NR are divided into three sections; that is,

$$f(x) = \begin{cases} G_b x + (G_a - G_b), & x > 1, \\ G_a x, & -1 \leq x \leq 1, \\ G_b x - (G_a - G_b), & x < -1, \end{cases} \quad (4)$$

$$= \begin{cases} -0.69x - 0.59, & x > 1, \\ -1.28x, & -1 \leq x \leq 1, \\ -0.69x + 0.59, & x < -1. \end{cases}$$

The three subspaces in the state space of (4) are

$$\begin{cases} D_1 = \{(x, y, z, w) \mid x > 1\}, \\ D_0 = \{(x, y, z, w) \mid -1 \leq x \leq 1\}, \\ D_{-1} = \{(x, y, z, w) \mid x < -1\}. \end{cases} \quad (5)$$

There are unique equilibrium points in three subspaces of the state space. The three unique equilibrium points are

$$\begin{aligned} P^+ &= (2.1388, 0.0738, -2.0650, 0.0738) \in D_1, \\ Q &= (0, 0, 0, 0) \in D_0, \\ P^- &= (-2.1388, -0.0738, 2.0650, -0.0738) \in D_{-1}. \end{aligned} \quad (6)$$

Linearization is carried out at the equilibrium point  $Q(0, 0, 0, 0)$ , and the linearization matrix is obtained as follows:

$$\begin{bmatrix} 2.8 & 10 & 0 & 0 \\ 1 & -1 & 1 & 0 \\ 0 & -16 & 0 & 16 \\ 0 & 0 & -0.05 & -1.4 \end{bmatrix}. \quad (7)$$

Four eigenvalues of the above matrix can be calculated:  $3.9298, -1.0103 + 3.3587i, -1.0103 - 3.3587i$ , and  $-1.5092$ ,

linearized at equilibrium points  $P^+$  and  $P^-$ , and the linearized matrix can be obtained as follows:

$$\begin{bmatrix} -3.1 & 10 & 0 & 0 \\ 1 & -1 & 1 & 0 \\ 0 & -16 & 0 & 16 \\ 0 & 0 & -0.05 & -1.4 \end{bmatrix}. \quad (8)$$

Four eigenvalues of the above matrix are calculated:  $-4.5531, 0.1295 + 3.4095i, 0.1295 - 3.4095i, -1.2060$ . Therefore, all equilibrium points  $P^+, Q$ , and  $P^-$  are saddle points. In the macroscopic view of chaotic attractors, holes are formed near  $P^+$  and  $P^-$ , respectively, which are like two whirlpools twisted together, showing a double-scroll chaotic strange attractor (Figure 3). This is the result of the combination of global stability and local instability. Chaotic orbits are the flow whirling around the strange attractor. The adjacent trajectories show a tendency of mutual exclusion and separation at an exponential rate [70].

There are many interesting chaotic phenomena when the system parameters are changed continuously. However, in order to debug the experimental circuit conveniently in the future, only the resistance  $R$  is changed to observe the  $x - y$  plane at the ends of  $C_1$  and  $C_2$ . In the simulation process, the  $x - y$  plane at the ends of  $C_1$  and  $C_2$  also shows that period-1 limit cycle, period-2 limit cycle, period-4 limit cycle, and single-band chaotic attractor are shown in Figure 5 and Table 1. It can be seen that the modified Chua's chaotic circuit exhibits abundant dynamic behavior of period doubling bifurcation sequence.

**2.2.2. Multistability Analysis.** Multistability allows flexibility of system performance without changing parameters, and appropriate control strategies can be used to induce switching behavior between different coexisting states. In order to study the complex dynamic characteristics of the system better, it is necessary to give some disturbance to the initial conditions, that is, to change the initial conditions of the system under the condition of keeping the system parameters unchanged. Figure 6 shows the coexistence phenomenon of the system under two different initial conditions. The initial condition of the blue trace is  $[0, 0.1, 0, 0]$  and the initial condition of the red trace is  $[0, -0.1, 0, 0]$ . It can be seen from Figure 6 that, under these two initial conditions, the attractors exhibited by the system are exactly the same, but the directions of the trajectories are different, which all depend on the symmetry of the system. Figure 6 shows the coexistence attractors for different parameter values  $\beta$  and  $\gamma_1$ . Figure 6(a) shows that the system has coexisting double-scroll chaotic attractors. Figure 6(b) shows that the system has coexisting single band chaotic attractors. Figure 6(c) shows that the system shows coexisting period-4 limit cycle. It is very interesting that Figure 6(d) shows that the system has a period-2 limit cycle coexistence phenomenon. Figure 6(e) shows that the system has a period-1 limit cycle coexistence phenomenon. Figure 6(f) is a time-domain waveform diagram of state  $x$ , and its parameter values are the same as period-1 limit cycle.

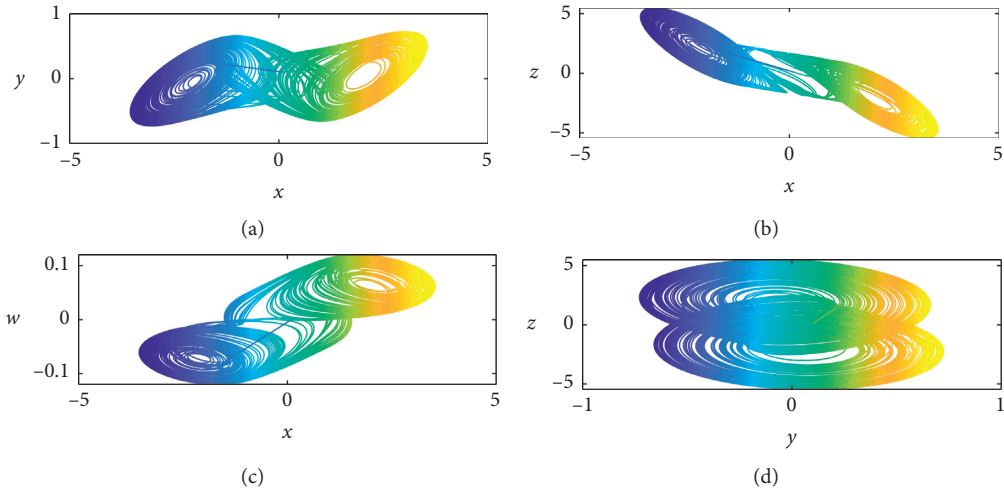


FIGURE 3: MATLAB simulation results of the modified Chua's chaotic circuit: (a) in  $x - y$  plane, (b) in  $x - z$  plane, (c) in  $x - w$  plane, and (d) in  $y - z$  plane.

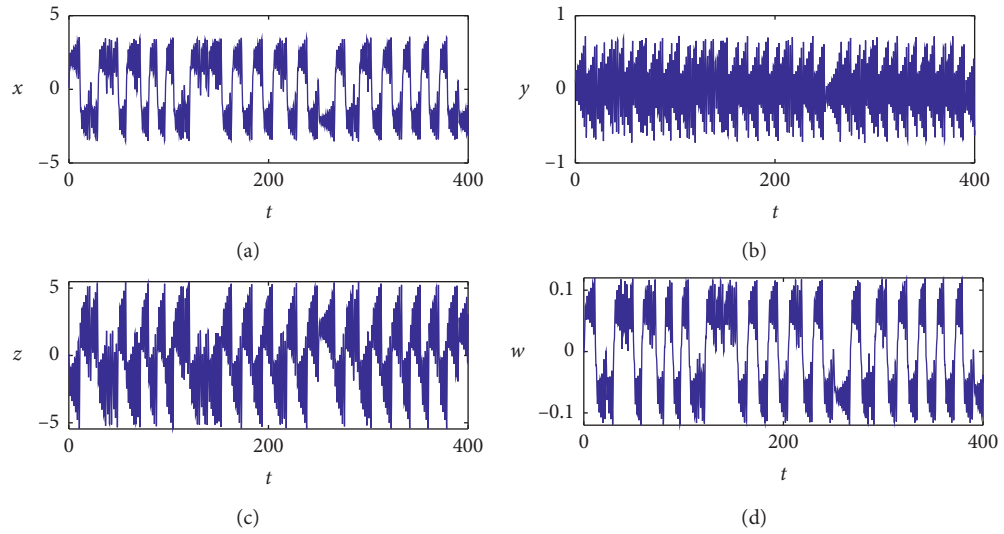


FIGURE 4: Time-domain waveforms of chaotic system (3).

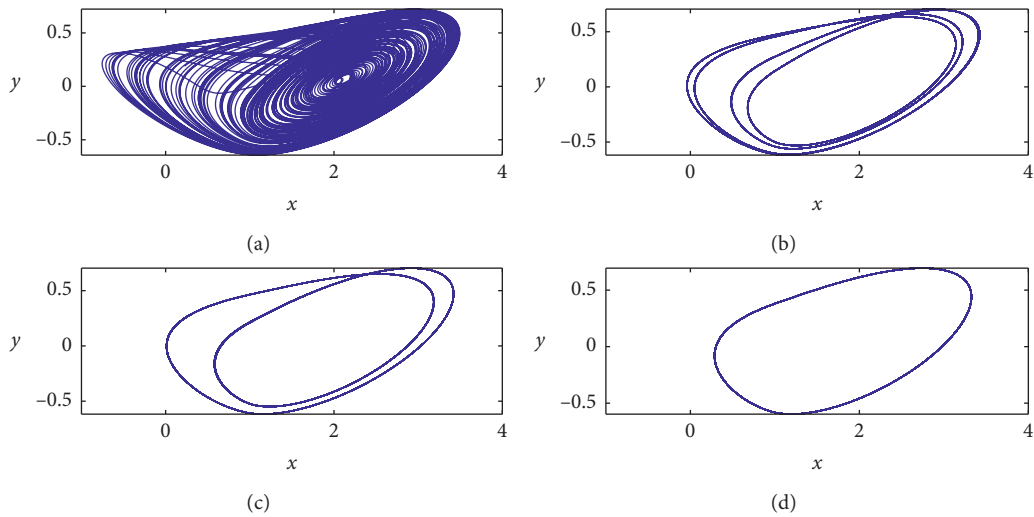


FIGURE 5: The period doubling scenario in the modified Chua's chaotic circuit shown in Figure 1: (a) single band chaotic attractor ( $R = 1734 \Omega$ ), (b) period-4 limit cycle ( $R = 1770 \Omega$ ), (c) period-2 limit cycle ( $R = 1775 \Omega$ ), and (d) period-1 limit cycle ( $R = 1801 \Omega$ ).

TABLE 1: Chaotic phenomena of the modified Chua's chaotic system by increasing resistance  $R$  values.

Chaotic phenomena	Range of $R$	$R$	$\alpha$	$\beta$	$\gamma_1$	$\gamma_2$	Figure
Single band chaotic attractor	1734 $\Omega$ –1769 $\Omega$	1734 $\Omega$	10	17.05	28.9	0.05	Figure 5(a)
Period-4 limit cycle	1770 $\Omega$ –1774 $\Omega$	1770 $\Omega$	10	17.76	29.5	0.05	Figure 5(b)
Period-2 limit cycle	1775 $\Omega$ –1800 $\Omega$	1775 $\Omega$	10	17.86	29.58	0.05	Figure 5(c)
Period-1 limit cycle	1801 $\Omega$ –1992 $\Omega$	1801 $\Omega$	10	18.39	30.02	0.05	Figure 5(d)

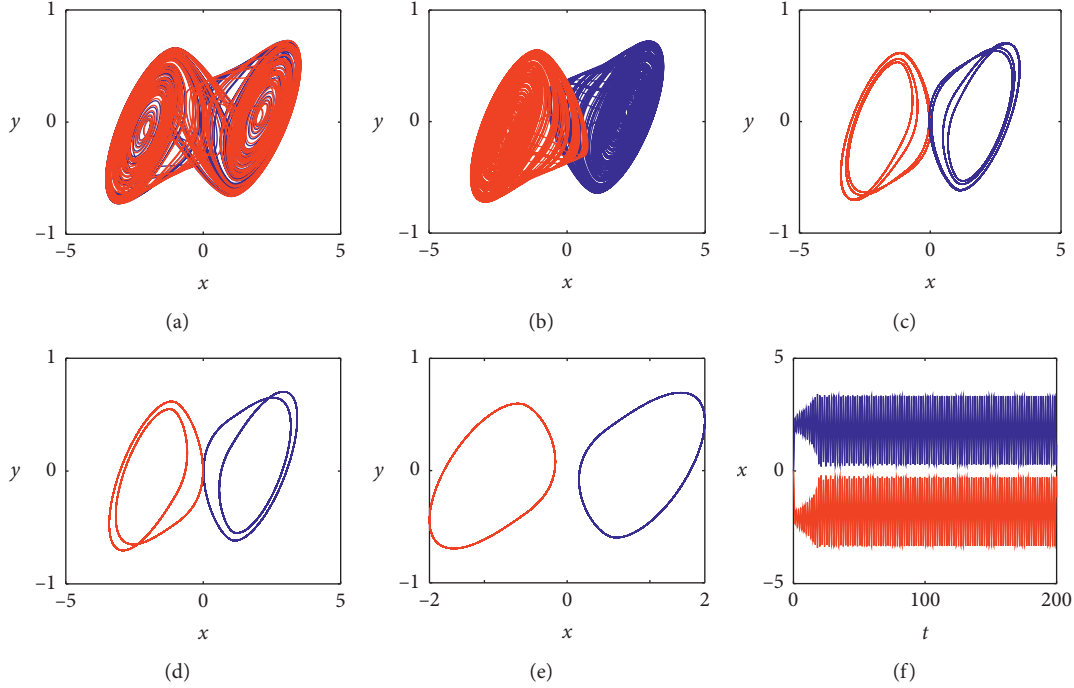


FIGURE 6: Coexisting attractors for the different parameter values  $\beta$  and  $\gamma_1$  and the initial conditions are  $[0, 0.1, 0, 0]$  and  $[0, -0.1, 0, 0]$  which are shown in blue and red, respectively: (a) coexisting double-scroll chaotic attractors, (b) coexisting single band chaotic attractors, (c) coexisting period-4 limit cycle, (d) coexisting period-2 limit cycle, (e) coexisting period-1 limit cycle, and (f) coexisting time-domain waveform diagram of state  $x$ .

### 3. Inductorless Modified Fourth-Order Autonomous Chua's Chaotic Circuit Based on CCII

3.1. *Inductorless Modified Chua's Chaotic Circuit Realized by CCII.* Current conveyor is a kind of electronic device with good high frequency performance, strong versatility, and flexibility, which has attracted wide attention of scholars [76–81]. In this part, a modified Chua's chaotic circuit realized by current conveyor is proposed. The key is to realize piecewise linear resistance  $NR$  and inductance  $L$  in Chua's chaotic circuit by using CCII commercial chip AD844 (current feedback operational amplifier) as the basic active device.

3.1.1. *CCII.* CCII is one of the most commonly used active devices in current-mode circuits. The symbolic representation of CCII is shown in Figure 7. Port relationship of CCII is

$$\begin{aligned} I_Y &= 0, \\ V_X &= V_Y, \\ I_Z &= KI_X, \end{aligned} \quad (9)$$

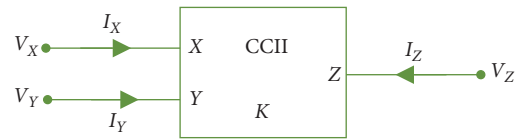


FIGURE 7: Symbolic representation of CCII.

where  $V_X$  and  $I_X$  are the voltage and current of  $X$ -terminal,  $V_Y$  and  $I_Y$  are the voltage and current of  $Y$ -terminal, and  $V_Z$  and  $I_Z$  are the voltage and current of  $Z$ -terminal, respectively.  $K$  is the transmission coefficient of the current conveyor. When  $K = 1$ , it is the in-phase current conveyor, and when  $K = -1$ , it is the reverse-phase current conveyor. The in-phase current conveyor can be implemented with one AD844, while the reverse-phase current conveyor needs two AD844. The implementation circuits are shown in Figures 8(a) and 8(b), respectively.

3.1.2. *Five-Segment Piecewise Nonlinear Resistance (NR).* Generally, when we use CCII to construct a nonlinear functional circuit, the five-segment piecewise nonlinear

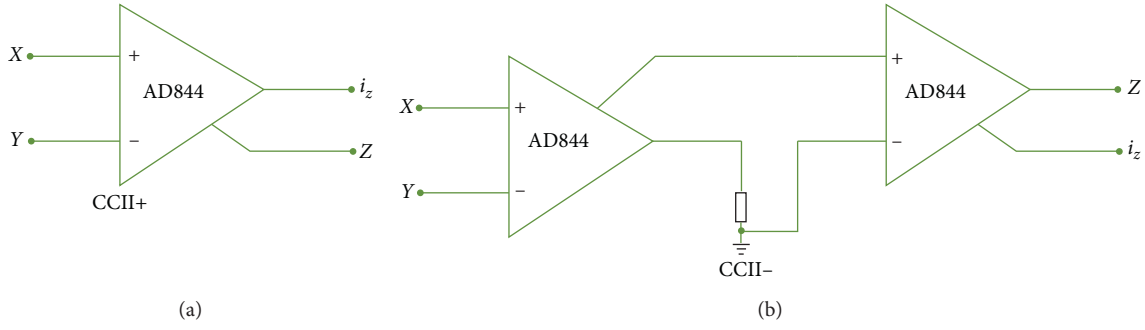


FIGURE 8: Implementation of the in-phase current conveyor (a) and the reverse-phase current conveyor (b).

resistance is employed. As shown in Figure 2, the input voltage is given to make it work in the middle of three BCDE segments. A five-piece nonlinear resistance [81] can be formed by parallel connection of two CCII, as shown in Figure 9(a). In Figure 2, the five-segment piecewise nonlinear resistance (NR)  $V$ - $I$  characteristic curve ABCDEF is generated by the circuit structure, the BCDE section has the characteristics of nonlinear negative resistance, and Chua's chaotic circuit mainly works in this curve section. The turning voltage and slope of the two circuits are  $E_a, E_b, G_a,$  and  $G_b,$  respectively. Therefore, the  $V$ - $I$  characteristic curve of the five-segment piecewise nonlinear resistance can be obtained as follows:

$$f(v) = \begin{cases} G_c v - (G_b - G_c)E_b - (G_a - G_b)E_a, & v < -E_b, \\ G_b v + (G_a - G_b)E_a, & -E_b \leq v < -E_a, \\ G_a v, & -E_a \leq v \leq E_a, \\ G_b v + (G_a - G_b)E_a, & E_a < v \leq E_b, \\ G_c v - (G_b - G_c)E_b - (G_a - G_b)E_a, & E_b < v. \end{cases} \quad (10)$$

According to the structure characteristics of the circuit shown in Figure 2, the slope expressions of each section are as follows:

$$\begin{aligned} E_a &= -R \left( \frac{1}{R_4} + \frac{1}{R_8} \right), \\ G_b &= R \left( \frac{1}{R_5} - \frac{1}{R_4} \right), \\ G_c &= R \left( \frac{1}{R_1} + \frac{1}{R_5} \right). \end{aligned} \quad (11)$$

The turning voltages of the circuit are

$$\begin{aligned} E_a &= \frac{R_8}{R_7 + R_8} V_{CC}, \\ E_b &= \frac{R_4}{R_3 + R_4} V_{CC}, \end{aligned} \quad (12)$$

where  $V_{CC}$  is the power supply voltage of the amplifier. Figure 9(b) shows the five-segment piecewise nonlinear resistance  $V$ - $I$  characteristic curve of Figure 9(a)'s circuit

which is simulated by Multisim. It can be seen that the curve is completely consistent with the performance of Figure 2.

**3.1.3. Lossless Grounded Active Inductor ( $L_{eq}$ ).** Although inductor is an important passive device in IC design, it is not easy to integrate because it cannot integrate itself. Therefore, spiral inductors are widely used in integrated circuits. Even so, there are some disadvantages, such as low adjustability, weight, large area, and high cost [82]. Therefore, in order to overcome these difficulties, inductance simulators are used as substitutes for spiral inductors in many circuit applications [97]. In this study, a lossless grounded active inductor based on CCII developed by Yang is used [81]. This is because CCII has proven to be very useful in either current or voltage-mode signal processing circuits. The principle circuit of the lossless grounded active inductor realized by CCII is shown in Figure 10.

In Figure 10, CCII-,  $Z_1,$  and  $Z_2$  form a voltage amplifier. CCII+,  $Z_2,$  and  $Z_3$  form a current amplifier. The input voltage  $v_i$  is added to the  $Y$ -terminal of CCII- and amplified by the voltage amplifier composed of CCII-,  $Z_1,$  and  $Z_2$ . According to the voltage-current relationship of CCII, if  $K = 1$ , the equivalent input impedance of the circuit shown in Figure 9(a) is

$$Z_{in} = \frac{Z_1 Z_2}{Z_3}. \quad (13)$$

It can be seen that the circuit shown in Figure 10 is an impedance converter, which can realize impedance conversion. By changing the properties of impedance  $Z_1, Z_2,$  and  $Z_3$ , different equivalent impedance can be obtained. If  $Z_1 = R_1, Z_2 = R_2,$  and  $Z_3 = 1/SC$ , the circuit can realize a lossless grounded active inductor, and the equivalent inductance value of the lossless grounded active inductor is

$$L_{eq} = R_1 R_2 C. \quad (14)$$

**3.1.4. Inductorless Modified Fourth-Order Autonomous Chua's Chaotic Circuit.** Figure 11 shows the modified Chua's chaotic circuit designed using CCII. The upper part inside the dash box of the circuit simulates a grounded inductor ( $L_{eq}$ ), the right part inside the dash box is piecewise five-segment linear NR designed using CCII, and the left

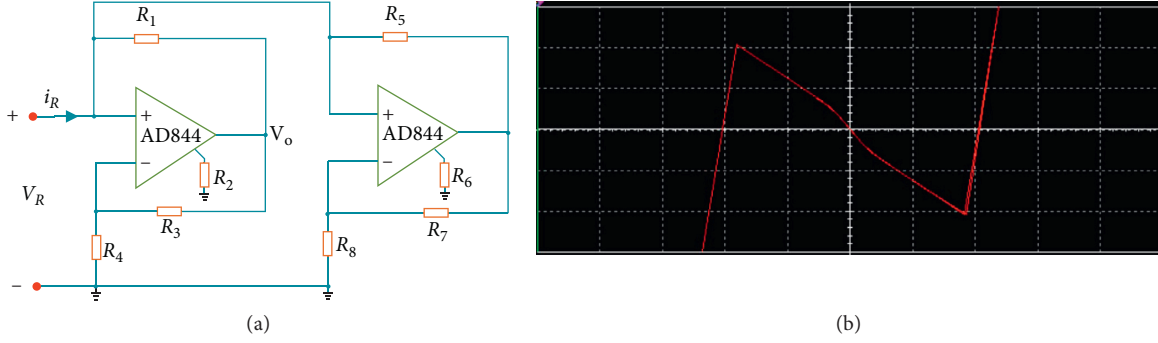


FIGURE 9: Five-segment piecewise nonlinear resistance implemented by two CCII: (a) circuit structure and (b)  $V$ - $I$  characteristic simulated by Multisim.

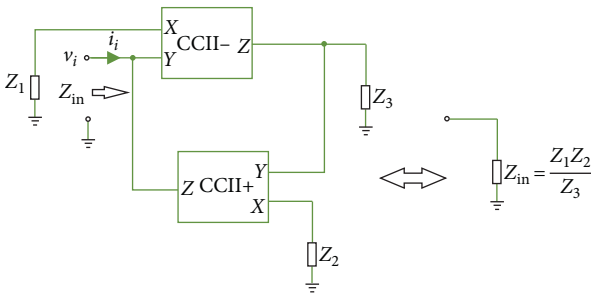


FIGURE 10: Lossless grounded active inductor circuit implemented by CCII.

part inside the dash box of the circuit is a linear RC network. The inspection of the present circuit configuration reveals that all the four state variables  $V_{C1}$ ,  $V_{C2}$ ,  $i_L$ , and  $V_{C3}$ , as stated in (1), are available from the circuit. The simulated inductance  $L_{eq}$  is composed of one CCII+, two CCII-, and one capacitor  $C_4$ . RC network is composed of  $C_1$ ,  $C_2$ ,  $C_3$ ,  $R_0$ , and  $R$ .  $C_2$ ,  $C_3$ , and  $L_{eq}$  constitute resonant circuit.  $C_1$  and piecewise linear resistance circuit are connected in parallel. Resistor  $R$  connects linear circuit and nonlinear circuit to form chaotic circuit. The values of components are taken in Table 2. This circuit is biased with  $\pm 15$  V supply. A double-scroll attractor is observed for  $R = 1680 \Omega$  as shown in Figure 12. Through the simulation of the circuit, we have also observed a variety of dynamic behaviors, such as single band chain attractor, period-4 limit cycle, period-2 limit cycle, period-1 limit cycle, steady state, and limit cycle, as shown in Figure 13. It can be seen that the Multisim simulation results are in good agreement with the theoretical analysis, which verifies the feasibility of the modified Chua's circuit.

#### 4. FPGA Implementation of the Multistable Modified Fourth-Order Autonomous Chua's Chaotic System

The multistable modified fourth-order autonomous Chua's chaotic system presented in this study is modeled on LabVIEW FPGA using Runge-Kutta (RK-4) algorithm, which is one of the most popular numerical differential equation decryption methods in the literature. According to the 32-bit IEEE 754-1985 floating-point number standard, the design is

coded on VHDL (Very-High-Speed High Speed Integrated Circuit Hardware Description Language) [98]. IP core generator developed by Vivado 2018.3 Design Tools system is used to design chaotic oscillator based on FPGA, such as multiplier, subtractor, and adder, which conform to IEEE 754-1985 standard.

**4.1. RK-4 Algorithm.** Runge-Kutta (RK) algorithm is a high precision one-step algorithm widely used in engineering. The theoretical basis of the algorithm is derived from Taylor's formula and the slope approximation to express the differential. It predicts the slope of several points several times in the integral interval, then carries out weighted averaging, which is used as the basis for the next point, and thus constructs a numerical integration calculation method with higher accuracy [90]. If the slopes of four points are calculated beforehand, it is the fourth-order Runge-Kutta (RK-4) algorithm. For differential equation  $\dot{y} = f(x, y)$ , the theoretical formula of RK-4 is as follows:

$$\begin{aligned}
 K1 &= f(x_k, y_k), \\
 K2 &= f\left(x_k + \frac{\Delta h}{2}, y_k + \frac{\Delta h}{2} K1\right), \\
 K3 &= f\left(x_k + \frac{\Delta h}{2}, y_k + \frac{\Delta h}{2} K2\right), \\
 K4 &= f(x_k + \Delta h, y_k + \Delta h K3), \\
 y_{k+1} &= y_k + \frac{\Delta h}{6} (K1 + 2K2 + 2K3 + K4),
 \end{aligned} \tag{15}$$

where  $K1, K2, K3, K4$  denote the first-order reciprocal of the output variable, that is, the differential at a point, expressed as the slope. The iteration step is  $\Delta h = 0.001$ . Figure 14 shows the block diagram of Chua's oscillator using RK-4 algorithm.  $x_0, y_0, z_0$ , and  $w_0$  signals are the initial conditions (IC) for the system to start running. In the design, they are defined as 32-bit symbolic floating-point numbers, which are determined internally by the user. The purpose of the multiplexer unit (MUX) is to select the external initial conditions at the

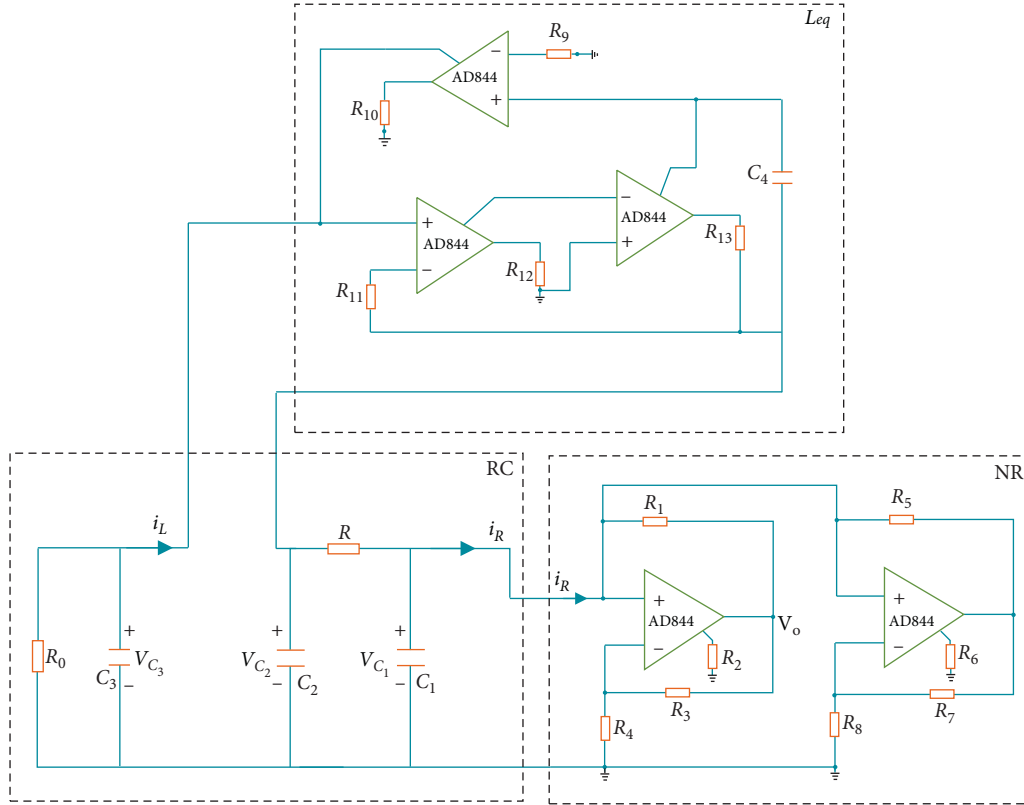


FIGURE 11: Inductorless modified Chua's chaotic circuit realized by CCII.

TABLE 2: Values of components used in the modified Chua's chaotic circuit.

Passive component	Value
$R_0$	60 $\Omega$
$R_1$	220 $\Omega$
$R_2$	220 $k\Omega$
$R_3$	220 $\Omega$
$R_4$	2.2 $k\Omega$
$R_5$	22 $k\Omega$
$R_6$	220 $k\Omega$
$R_7$	22 $k\Omega$
$R_8$	3.3 $k\Omega$
$R_9$	1 $k\Omega$
$R_{10}$	220 $k\Omega$
$R_{11}$	1 $k\Omega$
$R_{12}$	220 $k\Omega$
$R_{13}$	220 $k\Omega$
$R$	Variable
$C_1$	10 nF
$C_2$	100 nF
$C_3$	2 $\mu\text{F}$
$C_4$	17.64 nF

start or the internal values provided by the RK4-based oscillator unit in the successive steps. In the continuous steps after the start of operation, the  $x_{k+1}$ ,  $y_{k+1}$ ,  $z_{k+1}$ , and  $w_{k+1}$  signals generated by the oscillator unit are used as feedback inputs of the multiplexing unit, that is, the input signals of the next step, such as  $x_k$ ,  $y_k$ ,  $z_k$ , and  $w_k$ . The oscillator unit consists of six modules:  $K1$ ,  $K2$ ,  $K3$ ,  $K4$ ,  $ys$ , and filter, where

$K1$ ,  $K2$ ,  $K3$ ,  $K4$  modules are used to calculate the values of  $K1$ ,  $K2$ ,  $K3$ ,  $K4$  and  $ys$  module is used to calculate the value of  $x_{k+1}$ ,  $y_{k+1}$ ,  $z_{k+1}$ ,  $w_{k+1}$ . When  $ys$  does not produce the final required calculation results, the filter unit will prevent the intermediate value to reach the output.

**4.2. FPGA Implementation.** The top level block diagram of the modified fourth-order Chua's oscillator based on FPGA designed by RK-4 algorithm is shown in Figure 15. As can be seen from Figure 15, the design system has three inputs and five outputs. The input signal consists of a 1-bit clock signal (Clk), a 1-bit Reset, and a 32-bit  $\Delta h$ . Clk and Reset are used to ensure synchronization between the system and other modules. 32-bit  $\Delta h$  represents the step size, which is used to determine the sensitivity of the algorithm. The output signal consists of four 32-bit output signals  $X\_out$ ,  $Y\_out$ ,  $Z\_out$ ,  $W\_out$  and 1-bit flag signal  $XYZW\_ready$ . When the calculation generates  $X\_out$ ,  $Y\_out$ ,  $Z\_out$ ,  $W\_out$ , the flag signal  $XYZW\_ready$  is output.

The second level block diagram is composed of modified Chua's chaotic oscillator, floating-point to fixed-point unit, and digital-to-analog converter, as shown in Figure 16. The oscillator unit has three input signals, 1-bit Run, 1-bit Clk and 32-bit  $\Delta h$ , respectively. The 1-bit  $XYZW\_ready$  data signal provides the clock signal for the DAC unit. At the output of chaotic oscillator based on Rk-4, there are four floating-point standard 32-bit output signals ( $X\_out$ ,  $Y\_out$ ,  $Z\_out$ ,  $W\_out$ ). These signals are equivalent to the  $x$ ,  $y$ ,  $z$ , and  $w$  variables of the continuous-time chaotic system (3).

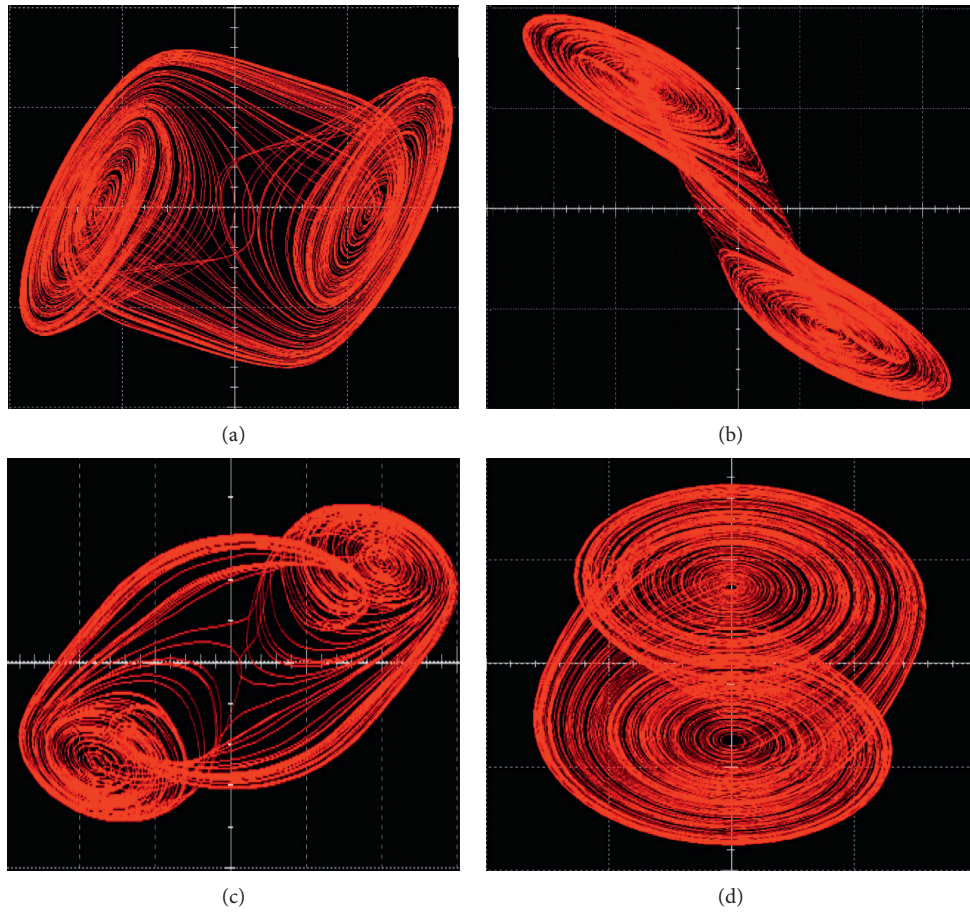


FIGURE 12: Multisim simulation of double-scroll phase portraits ( $R = 1680 \Omega$ ) of the inductorless modified Chua's chaotic circuit: (a) in  $x$ - $y$  plane, (b) in  $x$ - $z$  plane, (c) in  $x$ - $w$  plane, and (d) in  $y$ - $z$  plane.

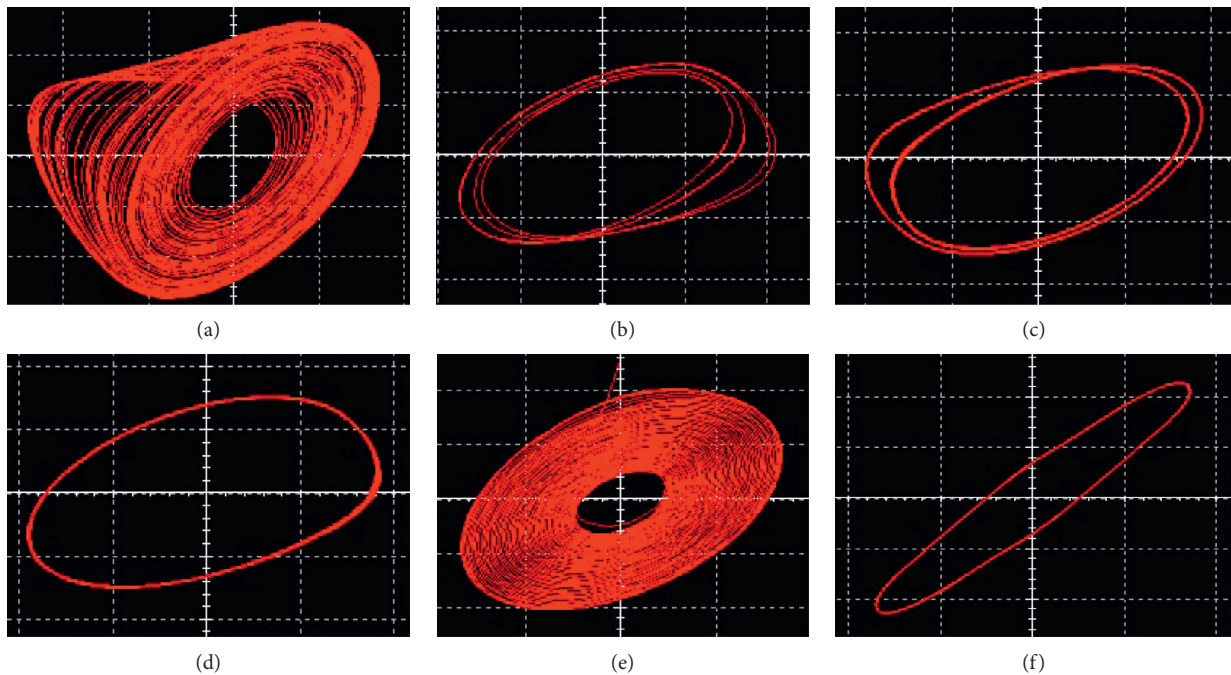


FIGURE 13: Multisim simulation of (a) single band chaotic attractor ( $R = 1950 \Omega$ ), (b) period-4 limit cycle ( $R = 1980 \Omega$ ), (c) period-2 limit cycle ( $R = 1990 \Omega$ ), (d) period-1 limit cycle ( $R = 2000 \Omega$ ), (e) steady state ( $R = 2040 \Omega$ ), and (f) limit cycle ( $R = 1100 \Omega$ ) in  $x$ - $y$  plane.

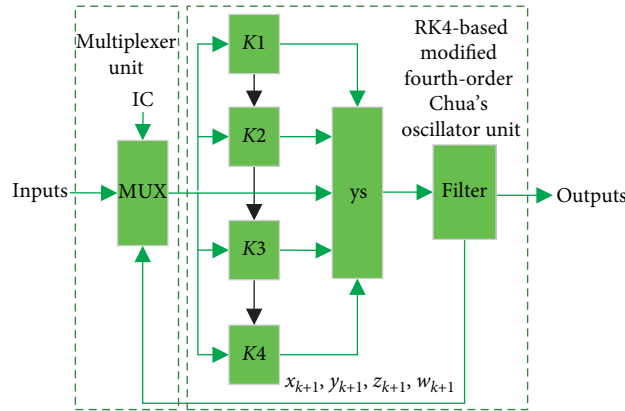


FIGURE 14: The block diagram of the FPGA-based multistable modified Chua's chaotic oscillator unit.

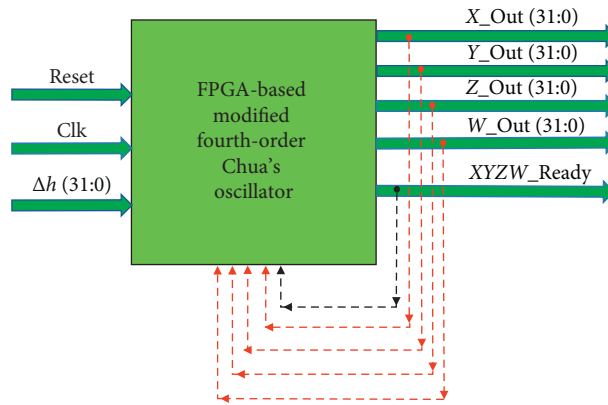


FIGURE 15: The top level block diagram of the FPGA-based multistable modified Chua's chaotic system.

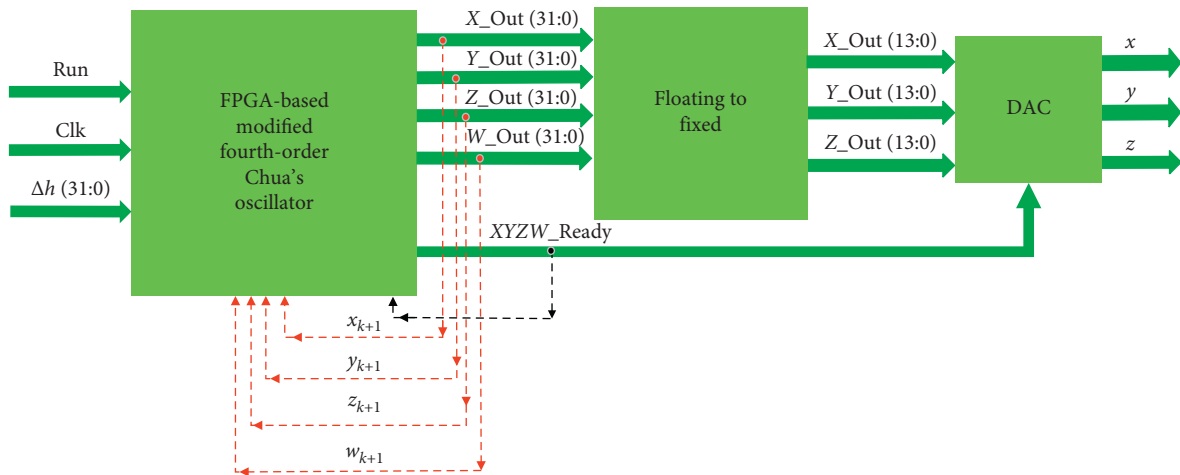


FIGURE 16: The second level block diagram of the FPGA-based multistable modified Chua's chaotic system.

The input of the floating-point to fixed-point unit is four 32-bit output signals of the oscillator unit, which converts the output of the former unit into 14-bit unsigned fixed-point. The DAC module converts the digital signal generated by the chaotic system into analog signal and outputs it to the oscilloscope. In the actual experiment, we choose

$X_{out}, Y_{out}$ , and  $Z_{out}$  to output the dual-channel DAC module and then the oscilloscope.

4.3. *FPGA Test Results.* The modified multistable fourth-order Chua's chaotic system based on RK-4 is synthesized on

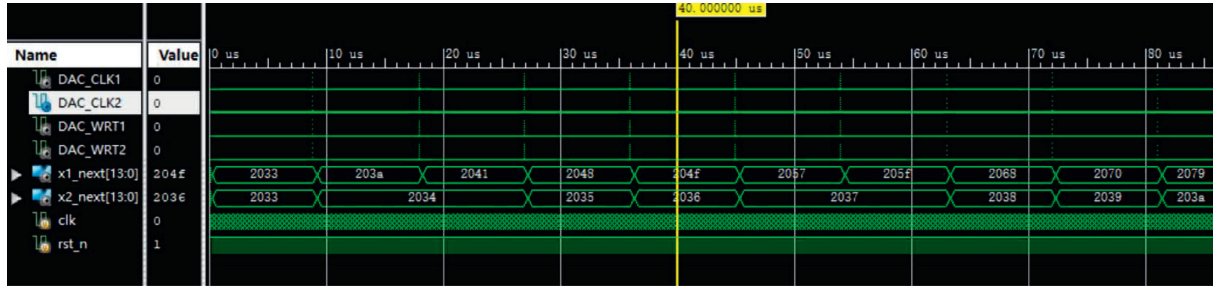


FIGURE 17: Xilinx ISim simulation results of the modified multistable fourth-order Chua's chaotic system based on FPGA.

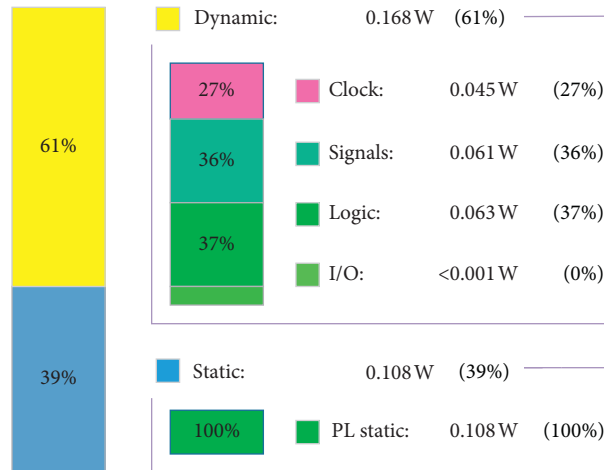


FIGURE 18: Power utilized by the system based on FPGA.

TABLE 3: The Xilinx ZYNQ-XC7Z020 chip statistics of FPGA-based multistable modified fourth-order Chua's chaotic system.

FPGA chip	Slice register number	LUTs number	Bonded IOBs number	Max. clock frequency (MHz)
ZYNQ-XC7Z020	21,711	16,430	34	180.180
Utilization (%)	20.01	30.88	27.20	—

Xilinx ZYNQ-XC7Z020 chip. The use of the chip source and the clock speed of the system are calculated. Using Vivado 2018.3 design tool, the data processing duration of the modified fourth-order Chua's chaotic system designed in this paper is determined. The  $X\_Out$ ,  $Y\_Out$ ,  $Z\_Out$ , and  $W\_Out$  signals are equivalent to the  $x$ ,  $y$ ,  $z$ , and  $w$  signals in the system. Although the 32-bit floating-point standard is adopted in the system design, which makes it easier to detect the time series values of these signals, the Vivado simulation results are displayed in hexadecimal digital format. The results of the Xilinx ISim simulator for the modified fourth-order Chua's chaotic system are shown in Figure 17 when  $\Delta h = 0.001$ . The system runs in pipeline mode and produces  $x$ ,  $y$ ,  $z$ , and  $w$  signals after every 320 clock cycles. Figure 18 shows the power utilized by the system. Table 3 shows the resources utilized by the chaotic oscillator implemented on FPGA including the clock frequency. The minimum working period of the modified fourth-order Chua's chaotic system signal generator based

on FPGA is 5.55 ns. Finally, the  $X\_Out$ ,  $Y\_Out$ , and  $Z\_Out$  signals obtained from the RK4-based FPGA design of the system are recorded in a file in the form of 32-bit floating-point hexadecimal number during the test step, which is given in Table 4. The phase portraits of the output signals are obtained using the data set generated in decimal format by the modified fourth-order Chua's chaotic system based on FPGA given in Table 4. Two pictures of the double-scroll chaotic attractors and single band chaotic attractor and period limit cycles obtained from the hardware implementation of the RK4-based modified fourth-order Chua's chaotic system on FPGA are shown in Figures 19 and 20, respectively. The results show that the phase portraits obtained by the model based on MATLAB and FPGA have good consistency. Although the implementation of FPGA has a reputation of being difficult to design, with the help of system methodology, the system can require less work than the traditional software-based implementation [99, 100].

TABLE 4: The conversion result from 32-bit floating-point number output by FPGA to decimal number.

FPGA output signals in 32-bit floating-point number with hexadecimal format			Decimal number values		
X_Out	Y_Out	Z_Out	$x(t)$	$y(t)$	$z(t)$
3ea6c5fa	3d8e688e	beb09da2	0.325729181065535	0.0695353589404750	-0.344952653576506
3eb5e9f5	3d8b58d6	beba7076	0.355300589372080	0.0680405320103716	-0.364139270662248
3ea6c5fa	3d8e688e	beb09da2	0.325729181065535	0.0695353589404750	-0.344952653576506
3f80921f	3db1af46	bf22ec49	1.00445926841886	0.0867600901838271	-0.636417953148042
3f818177	3db2d8e2	bf239408	1.01176345370630	0.0873277341857656	-0.638977523652504
400097f8	3e6cb53e	bfc2f4b9	2.00927537971617	0.231160129151098	-1.52309338070114
4002b408	3e70defb	bfca54f4	2.04223825024841	0.235225603385658	-1.58071756451930
4004bed6	3e748682	bfd1cf6d	2.07414771146939	0.238794362382855	-1.63914268012843
404d076a	3efe07f0	c0686855	3.20357746761604	0.496154299792244	-3.63136802769324
404de8cc	3ef5d30f	c06fb384	3.21733377662411	0.480125878954796	-3.74533166924290
404e9294	3eecea3c	c076ae83	3.22769634415875	0.462724565296702	-3.85440145110143
bf806354	bd80f4ae	400d650e	-1.00303124071647	-0.0629666870295447	2.20929280483211

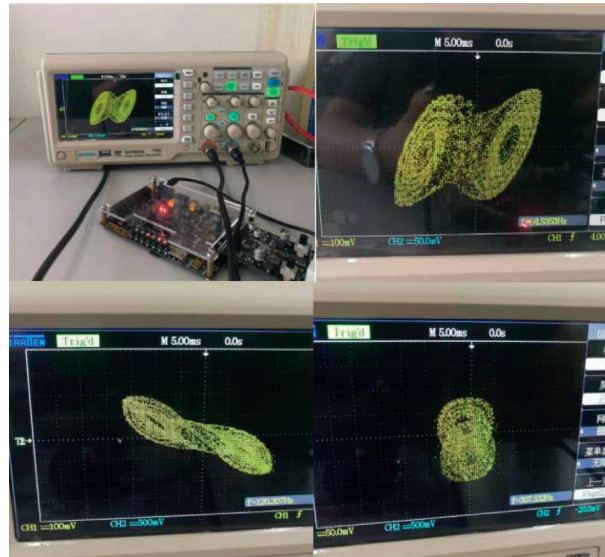


FIGURE 19: Implementation platform and exemplification of the double-scroll chaotic attractors generated by the FPGA implementation of the multistable modified fourth-order Chua’s chaotic system.

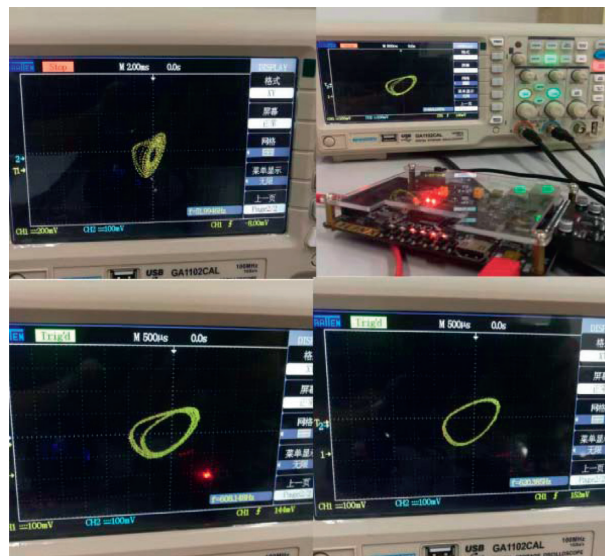


FIGURE 20: Implementation platform and exemplification of the single band chaotic attractor and period limit cycles generated by the FPGA implementation of the multistable modified fourth-order Chua’s chaotic system.

## 5. Conclusion

A multistable modified fourth-order autonomous Chua's chaotic system is first investigated. Then the modified implementation of fourth-order autonomous Chua's chaotic circuit with CCII based active elements and synthetic inductor is reported. Synthetic inductor instead of the inductor coil makes the circuit more suitable for the fabrication of integrated circuits, which can be used for the study of coupled dynamics and spatiotemporal chaos. The modified Chua's circuit exhibits abundant dynamic behavior of period doubling bifurcation sequence. Finally, the design of multistable modified fourth-order autonomous Chua's chaotic system based on discrete-time FPGA is implemented on Xilinx Virtex-6 (ZYNQ-XC7Z020) chip using RK-4 algorithm. The maximum operating frequency of the designed chaotic system reaches 180.180 MHz. As can be observed from the results, the chaotic signal generator based on FPGA proposed in this paper can be used as a good entropy source in the applications of secure communication, cryptosystem, and random number generator.

## Data Availability

All data used to support the findings of this study are available from the corresponding authors upon request.

## Conflicts of Interest

The authors declare that they have no conflicts of interest.

## Acknowledgments

This work was partly supported by the National Natural Science Foundation of China under Grants 61504013, 61702052, 61772087, 61674054, and 61801054, the Natural Science Foundation of Hunan Province under Grants 2019JJ50648, 2016jj2005, 2017JJ2049, and 2017JJ3254, the Scientific Research Foundation of Hunan Provincial Education Department under Grants 18A137, 16B212, and 17C0048, and the National Key Research and Development Project under Grant 2018YFE0111200.

## References

- [1] H. Lin and C. Wang, "Influences of electromagnetic radiation distribution on chaotic dynamics of a neural network," *Applied Mathematics and Computation*, vol. 369, p. 124840, 2020.
- [2] F. Tan, L. Zhou, F. Yu, and J. Lu, "Fixed-time continuous stochastic synchronisation of two-layer dynamical networks," *International Journal of Systems Science*, vol. 51, no. 2, pp. 242–257, 2019.
- [3] J. Jin, L. Zhao, M. Li, F. Yu, and Z. Xi, "Improved zeroing neural networks for finite time solving nonlinear equations," *Neural Computing and Applications*, 2019.
- [4] F. Yu, L. Liu, L. Xiao, K. Li, and S. Cai, "A robust and fixed-time zeroing neural dynamics for computing time-variant nonlinear equation using a novel nonlinear activation function," *Neurocomputing*, vol. 350, pp. 108–116, 2019.
- [5] L. Zhou, F. Tan, F. Yu, and W. Liu, "Cluster synchronization of two-layer nonlinearly coupled multiplex networks with multi-links and time-delays," *Neurocomputing*, vol. 359, pp. 264–275, 2019.
- [6] F. Wang, L. Zhang, S. Zhou, and Y. Huang, "Neural network-based finite-time control of quantized stochastic nonlinear systems," *Neurocomputing*, vol. 362, pp. 195–202, 2019.
- [7] L. Xiang, G. Guo, and J. Yu, "A convolutional neural network-based linguistic steganalysis for synonym substitution steganography," *Mathematical Biosciences and Engineering*, vol. 17, no. 2, pp. 1041–1058, 2020.
- [8] C. Wang, L. Xiong, J. Sun, and W. Yao, "Memristor-based neural networks with weight simultaneous perturbation training," *Nonlinear Dynamics*, vol. 95, no. 4, pp. 2893–2906, 2019.
- [9] W. Yao, C. Wang, J. Cao, Y. Sun, and C. Zhou, "Hybrid multisynchronization of coupled multistable memristive neural networks with time delays," *Neurocomputing*, vol. 363, pp. 281–294, 2019.
- [10] L. Zhou, C. Wang, and L. Zhou, "A novel no-equilibrium hyperchaotic multi-wing system via introducing memristor," *International Journal of Circuit Theory and Applications*, vol. 46, no. 1, pp. 84–98, 2018.
- [11] F. Yu, L. Liu, S. Qian et al., "Chaos-based application of a novel multistable 5D memristive hyperchaotic system with coexisting multiple attractors," *Complexity*, vol. 2020, Article ID 8034196, 2020.
- [12] J. Jin, "Programmable multi-direction fully integrated chaotic oscillator," *Microelectronics Journal*, vol. 75, pp. 27–34, 2018.
- [13] L. Zhou, C. Wang, X. Zhang, and W. Yao, "Various attractors, coexisting attractors and antimonotonicity in a simple fourth-order memristive twin-T oscillator," *International Journal of Bifurcation and Chaos*, vol. 28, no. 4, Article ID 1850050, 2018.
- [14] Q. Zhao, C. H. Wang, and X. Zhang, "A universal emulator for memristor, memcapacitor, and meminductor and its chaotic circuit," *Chaos*, vol. 29, Article ID 013141, 2019.
- [15] F. Yu, S. Qian, X. Chen et al., "A new 4D four-wing memristive hyperchaotic system: dynamical analysis, electronic circuit design, shape synchronization and secure communication," *International Journal of Bifurcation and Chaos*, 2020.
- [16] G. Cheng, C. Wang, and H. Chen, "A novel color image encryption algorithm based on hyperchaotic system and permutation-diffusion architecture," *International Journal of Bifurcation and Chaos*, vol. 29, no. 9, Article ID 1950115, 2019.
- [17] Y. Chen, J. Wang, R. Xia, Q. Zhang, Z. Cao, and K. Yang, "The visual object tracking algorithm research based on adaptive combination kernel," *Journal of Ambient Intelligence and Humanized Computing*, vol. 10, no. 12, pp. 4855–4867, 2019.
- [18] Y. Chen, J. Xiong, W. Xu, and J. Zuo, "A novel online incremental and decremental learning algorithm based on variable support vector machine," *Cluster Computing*, vol. 22, no. S3, pp. 7435–7445, 2019.
- [19] F. Peng, X. W. Zhu, and M. Long, "An ROI privacy protection scheme for H.264 video based on FMO and chaos," *IEEE Transactions on Information Forensics and Security*, vol. 8, pp. 1688–1699, 2013.
- [20] Y. Chen, J. Wang, X. Chen et al., "Single-image super-resolution algorithm based on structural self-similarity and deformation block features," *IEEE Access*, vol. 7, pp. 58791–58801, 2019.

- [21] S. Wang, C. Wang, and C. Xu, "An image encryption algorithm based on a hidden attractor chaos system and the Knuth-Durstenfeld algorithm," *Optics and Lasers in Engineering*, vol. 128, Article ID 105995, 2020.
- [22] C. K. Volos, V. Sundarapandian, P. Viet-Thanh et al., "Discrete chaotic dynamics for economics and social science," *Discrete Dynamics in Nature and Society*, vol. 2016, no. 2, Article ID 3105084, 2016.
- [23] J. Jin and L. Zhao, "Low voltage low power fully integrated chaos generator," *Journal of Circuits, Systems and Computers*, vol. 27, no. 10, Article ID 1850155, 2018.
- [24] J. Jin and L. Cui, "Fully integrated memristor and its application on the scroll-controllable hyperchaotic system," *Complexity*, vol. 2019, no. 8, Article ID 4106398, 2019.
- [25] F. Yu, L. Gao, K. Gu, B. Yin, Q. Wan, and Z. Zhou, "A fully qualified four-wing four-dimensional autonomous chaotic system and its synchronization," *Optik*, vol. 131, pp. 79–88, 2017.
- [26] X. Zhang, C. Wang, W. Yao, and H. Lin, "Chaotic system with bondorbital attractors," *Nonlinear Dynamics*, vol. 97, no. 4, pp. 2159–2174, 2019.
- [27] C. Wang, X. Liu, and H. Xia, "Multi-piecewise quadratic nonlinearity memristor and its  $2N$ -scroll and  $2N + 1$ -scroll chaotic attractors system," *Chaos*, vol. 27, Article ID 033114, 2017.
- [28] X. Zhang and C. Wang, "Multiscroll hyperchaotic system with hidden attractors and its circuit implementation," *International Journal of Bifurcation and Chaos*, vol. 29, no. 9, Article ID 1950117, 2019.
- [29] K. Christos, S. J. Volos, K. Jacques et al., "Nonlinear dynamics and entropy of complex systems with hidden and self-excited attractors," *Entropy*, vol. 21, p. 370, 2019.
- [30] T. Hayat, F. Masood, S. Qayyum et al., "Entropy generation minimisation: nonlinear mixed convective flow of Sisko nanofluid," *Pramana*, vol. 93, p. 96, 2019.
- [31] M. Zhou and C. Wang, "A novel image encryption scheme based on conservative hyperchaotic system and closed-loop diffusion between blocks," *Signal Processing*, vol. 171, Article ID 107484, 2020.
- [32] K. Gu, X. Dong, and L. Wang, "Efficient traceable ring signature scheme without pairings," *Advances in Mathematics of Communications*, 2019.
- [33] Z. Xia, Z. Fang, F. Zou et al., "Research on defensive strategy of real-time price attack based on multiperson zero-determinant," *Security and Communication Networks*, vol. 2019, Article ID 6956072, 13 pages, 2019.
- [34] K. Gu, K. Wang, and L. Yang, "Traceable attribute-based signature, journal of information security and applications," *Journal of Information Security and Applications*, vol. 49, pp. 1–16, 2019.
- [35] L. Xiang, Y. Li, W. Hao, P. Yang, and X. Shen, "Reversible natural language watermarking using synonym substitution and arithmetic coding," *CMC: Computers, Materials & Continua*, vol. 55, pp. 541–559, 2018.
- [36] K. Gu, W. Jia, J. Zhang et al., "Identity-based multi-proxy signature scheme in the standard model," *Fundamenta Informaticae*, vol. 150, no. 2, pp. 179–210, 2017.
- [37] K. Gu, N. Wu, B. Yin et al., "Secure data sequence query framework based on multiple fogs," *IEEE Transactions on Emerging Topics in Computing*, 2019.
- [38] K. Gu, N. Wu, B. Yin et al., "Secure data query framework for cloud and fog computing," *IEEE Transactions on Network and Service Management*, 2019.
- [39] K. Gu, W. Jia, G. Wang, and S. Wen, "Efficient and secure attribute-based signature for monotone predicates," *Acta Informatica*, vol. 54, no. 5, pp. 521–541, 2017.
- [40] Y. Chen, J. Wang, S. Liu et al., "Multiscale fast correlation filtering tracking algorithm based on a feature fusion model," *Concurrency and Computation: Practice and Experience*, 2019.
- [41] K. Gu, W. Zhang, S.-J. Lim, P. K. Sharma, Z. Al-Makhadmeh, and A. Tolba, "Reusable mesh signature scheme for protecting identity privacy of IoT devices," *Sensors*, vol. 20, no. 3, p. 758, 2020.
- [42] Z. Liu, Z. Lai, W. Ou, W. Ou, K. Zhang, and R. Zheng, "Structured optimal graph based sparse feature extraction for semi-supervised learning," *Signal Processing*, vol. 170, Article ID 107456, 2020.
- [43] L. Zhou and F. Tan, "A chaotic secure communication scheme based on synchronization of double-layered and multiple complex networks," *Nonlinear Dynamics*, vol. 96, no. 2, pp. 869–883, 2019.
- [44] F. Yu and C. Wang, "Secure communication based on a four-wing chaotic system subject to disturbance inputs," *Optik*, vol. 125, no. 20, pp. 5920–5925, 2014.
- [45] F. Yu, L. Li, Q. Tang et al., "A survey on true random number generators based on chaos," *Discrete Dynamics in Nature and Society*, vol. 2019, Article ID 2545123, 10 pages, 2019.
- [46] F. Yu, Q. Wan, J. Jin et al., "Design and FPGA implementation of a pseudorandom number generator based on a four-wing memristive hyperchaotic system and Bernoulli map," *IEEE Access*, vol. 7, pp. 181884–181898, 2019.
- [47] L. Zhou, F. Tan, and F. Yu, "A robust synchronization-based chaotic secure communication scheme with double-layered and multiple hybrid networks," *IEEE Systems Journal*, 2019.
- [48] F. Yu, C. Wang, Q. Wan, and Y. Hu, "Complete switched modified function projective synchronization of a five-term chaotic system with uncertain parameters and disturbances," *Pramana*, vol. 80, no. 2, pp. 223–235, 2013.
- [49] F. Yu and Y. Song, "Complete switched generalized function projective synchronization of a class of hyperchaotic systems with unknown parameters and disturbance inputs," *Journal of Dynamic Systems, Measurement, and Control-Transactions of the ASME*, vol. 136, Article ID 014505, 2014.
- [50] B.-C. Lai and J.-J. He, "Dynamic analysis, circuit implementation and passive control of a novel four-dimensional chaotic system with multiscroll attractor and multiple coexisting attractors," *Pramana*, vol. 90, p. 33, 2018.
- [51] S. T. Kingni, J. R. M. Pone, G. F. Kuate et al., "Coexistence of attractors in integer- and fractional-order three-dimensional autonomous systems with hyperbolic sine nonlinearity: analysis, circuit design and combination synchronization," *Pramana*, vol. 93, p. 12, 2019.
- [52] Q. Deng and C. Wang, "Multi-scroll hidden attractors with two stable equilibrium points," *Chaos*, vol. 29, Article ID 093112, 2019.
- [53] F. Yu, C. Wang, and H. He, "Grid multiscroll hyperchaotic attractors based on Colpitts oscillator mode with controllable grid gradient and scroll numbers," *Journal of Applied Research and Technology*, vol. 11, no. 3, pp. 371–380, 2013.
- [54] F. Yu, L. Liu, B. He et al., "Analysis and FPGA realization of a novel 5D hyperchaotic four-wing memristive system, active control synchronization, and secure communication application," *Complexity*, vol. 2019, Article ID 4047957, 18 pages, 2019.
- [55] C. Wang, L. Zhou, and R. Wu, "The design and realization of a hyper-chaotic circuit based on a flux-controlled memristor with linear memductance," *Journal of Circuits, Systems and Computers*, vol. 27, no. 3, Article ID 1850038, 2018.
- [56] A. R. Vazquez and M. D. Restituto, "CMOS design of chaotic oscillator using state variables: a monolithic Chua's circuit,"

- IEEE Transactions on Circuits and Systems*, vol. 40, pp. 596–612, 1993.
- [57] Q. Xu, Y. Lin, B. Bao, and M. Chen, “Multiple attractors in a non-ideal active voltage-controlled memristor based Chua’s circuit,” *Chaos, Solitons & Fractals*, vol. 83, pp. 186–200, 2016.
- [58] L. O. Chua, M. Komuro, and T. Matsumoto, “The double scroll family,” *IEEE Transactions on Circuits and Systems*, vol. 33, pp. 1073–1118, 1986.
- [59] C. X. Liu, “Analysis of Chua’s dual chaotic circuit,” *Acta Physica Sinica*, vol. 51, pp. 1198–1202, 2002.
- [60] M. Z. D. I. Hoz, L. Acho, Y. Vidal et al., “A modified Chua chaotic oscillator and its application to secure communications,” *Applied Mathematics and Computation*, vol. 247, pp. 712–722, 2014.
- [61] D. Chen, Z. Sun, X. Ma, and L. Chen, “Circuit implementation and model of a new multi-scroll chaotic system,” *International Journal of Circuit Theory and Applications*, vol. 42, no. 4, pp. 407–424, 2014.
- [62] G. Gandhi, “An improved Chua’s circuit and its use in hyperchaotic circuit,” *Analog Integrated Circuits and Signal Processing*, vol. 46, no. 2, pp. 173–178, 2006.
- [63] B. Bao, T. Jiang, G. Wang, P. Jin, H. Bao, and M. Chen, “Two-memristor-based Chua’s hyperchaotic circuit with plane equilibrium and its extreme multistability,” *Nonlinear Dynamics*, vol. 89, no. 2, pp. 1157–1171, 2017.
- [64] A. T. Azar, N. M. Adele, K. S. T. Alain et al., “Multistability analysis and function projective synchronization in relay coupled oscillators,” *Complexity*, vol. 2018, Article ID 3286070, 12 pages, 2018.
- [65] M. Chen, Y. Feng, H. Bao et al., “Hybrid state variable incremental integral for reconstructing extreme multistability in memristive jerk system with cubic nonlinearity,” *Complexity*, vol. 2019, Article ID 8549472, 16 pages, 2019.
- [66] Y. Zhang, Z. Liu, M. Chen et al., “Dimensionality reduction reconstitution for extreme multistability in memristor-based Colpitts system,” *Complexity*, vol. 2019, Article ID 4308549, 12 pages, 2019.
- [67] H. Bao, T. Jiang, K. Chu et al., “Memristor-based canonical chuas circuit: extreme multistability in voltage-current domain and its controllability in flux-charge domain,” *Complexity*, vol. 2018, Article ID 5935637, 13 pages, 2018.
- [68] Y. Qian and W. Meng, “Mixed-mode oscillation in a class of delayed feedback system and multistability dynamic response,” *Complexity*, vol. 2020, Article ID 4871068, 18 pages, 2020.
- [69] F. Yu, Z. Zhang, L. Liu et al., “Secure communication scheme based on a new 5D multistable four-wing memristive hyperchaotic system with disturbance inputs,” *Complexity*, vol. 2019, Article ID 5859273, 16 pages, 2019.
- [70] X. Luo, L. Huo, and G. Zhang, “Chaos characteristics based on modified Chua’s circuit,” *Journal of Chongqing Technology and Business University (Natural Science Edition)*, vol. 24, pp. 65–68, 2007.
- [71] C. L. Koliopoulos, I. M. Kyprianidis, I. N. Stouboulos, A. N. Anagnostopoulos, and L. Magafas, “Chaotic behaviour of a fourth-order autonomous electric circuit,” *Chaos, Solitons & Fractals*, vol. 16, no. 2, pp. 173–182, 2003.
- [72] X. Liu, J. Wang, and L. Huang, “Attractors of fourth-order Chua’s circuit and chaos control,” *International Journal of Bifurcation and Chaos*, vol. 17, no. 8, pp. 2705–2722, 2007.
- [73] C. H. Wang, H. Xu, and F. Yu, “A novel approach for constructing high-order Chua’s circuit with multi-directional multi-scroll chaotic attractors,” *International Journal of Bifurcation and Chaos*, vol. 23, p. 50022, 2013.
- [74] R. Bhattacharya, A. Basu, and S. K. Koul, “A highly linear CMOS active inductor and its application in filters and power dividers,” *IEEE Microwave and Wireless Components Letters*, vol. 25, no. 11, pp. 715–717, 2015.
- [75] G. Leuzzi, V. Stornelli, and S. Del Re, “A tuneable active inductor with high dynamic range for band-pass filter applications,” *IEEE Transactions on Circuits and Systems II: Express Briefs*, vol. 58, no. 10, pp. 647–651, 2011.
- [76] X. Zhang and C. Wang, “A novel multi-attractor period multi-scroll chaotic integrated circuit based on CMOS wide adjustable CCCII,” *IEEE Access*, vol. 7, pp. 16336–16350, 2019.
- [77] L. Zhao and C. H. Wang, “A novel CMOSCCCII based on cross-coupled differential transistor pair and its application,” *Wireless Personal Communications*, vol. 85, no. 4, pp. 2295–2307, 2015.
- [78] Y. Lin, C. Wang, and H. He, “A simple multi-scroll chaotic oscillator employing CCII,” *Optik*, vol. 126, no. 7–8, pp. 824–827, 2015.
- [79] Y. Lin and C. Wang, “Current-mode multi-scroll chaos generator employing CCCII,” *Electronics Letters*, vol. 52, no. 15, pp. 1295–1297, 2016.
- [80] F. Yu, P. Li, K. Gu, and B. Yin, “Research progress of multi-scroll chaotic oscillators based on current-mode devices,” *Optik*, vol. 127, no. 13, pp. 5486–5490, 2016.
- [81] Z. M. Yang, J. Z. hang, and J. Y. Ma, “Design and realization of Chua’s circuit based on current conveyers, et al,” *Acta Physica Sinica*, vol. 59, pp. 3007–3016, 2010.
- [82] R. Jothimurugan, K. Suresh, P. M. Ezhilarasu, and K. Thamilmaran, “Improved realization of canonical Chua’s circuit with synthetic inductor using current feedback operational amplifiers,” *AEU—International Journal of Electronics and Communications*, vol. 68, no. 5, pp. 413–421, 2014.
- [83] F. Yu, Q. Tang, W. Wang, and H. Wu, “A 2.7 GHz low-phase-noise LC-QVCO using the gate-modulated coupling technique,” *Wireless Personal Communications*, vol. 86, no. 2, pp. 671–681, 2016.
- [84] F. Yu, “A low-voltage and low-power 3-GHz CMOS LC VCO for S-band wireless applications,” *Wireless Personal Communications*, vol. 78, no. 2, pp. 905–914, 2014.
- [85] J. Jin and M. Tan, “Low power quadrature voltage controlled oscillator,” *International Journal of RF and Microwave Computer-Aided Engineering*, vol. 29, no. 12, 2019.
- [86] Q. Wan, J. Dong, H. Zhou, and F. Yu, “A very low power quadrature VCO with modified current-reuse and back-gate coupling topology,” *Journal of Circuits, Systems and Computers*, vol. 26, no. 11, p. 1750184, 2017.
- [87] F. Yu, L. Gao, L. Liu, S. Qian, S. Cai, and Y. Song, “A 1 V, 0.53 ns, 59  $\mu$ W current comparator using standard 0.18  $\mu$ m CMOS technology,” *Wireless Personal Communications*, 2019.
- [88] S. Penaud, J. Guittard, PBouysse et al., “DSP implementation of self-synchronised chaotic encoder-decoder,” *Electronics Letters*, vol. 36, pp. 365–366, 2002.
- [89] R. M. Hidalgo, J. G. Fernández, R. R. Rivera, and H. A. Larrondo, “Versatile DSP-based chaotic communication system,” *Electronics Letters*, vol. 37, no. 19, pp. 1204–1205, 2001.
- [90] İ. Koyuncu and A. Turan Özcerit, “The design and realization of a new high speed FPGA-based chaotic true random number generator,” *Computers & Electrical Engineering*, vol. 58, pp. 203–214, 2017.
- [91] M. Tuna, M. Alçın, İ. Koyuncu, C. B. Fidan, and İ. Pehlivan, “High speed FPGA-based chaotic oscillator design,” *Microprocessors and Microsystems*, vol. 66, pp. 72–80, 2019.

- [92] M. Alcin, I. Pehlivan, I. Koyuncu et al., "Hardware design and implementation of a novel ANN-based chaotic generator in FPGA," *Optik*, vol. 127, pp. 5500–5505, 2016.
- [93] A. Akgul, H. Calgan, I. Koyuncu, I. Pehlivan, and A. Istanbulu, "Chaos-based engineering applications with a 3D chaotic system without equilibrium points," *Nonlinear Dynamics*, vol. 84, no. 2, pp. 481–495, 2016.
- [94] Q. Lai, X. W. Zhao, K. Rajagopa et al., "FPGA implementation and engineering applications of multi-butterfly chaotic attractors generated from generalized Sprott C system," *Pramana*, vol. 90, p. 6, 2018.
- [95] J.-L. Zhang, W.-Z. Wang, X.-W. Wang, and Z.-H. Xia, "Enhancing security of FPGA-based embedded systems with combinational logic binding," *Journal of Computer Science and Technology*, vol. 32, no. 2, pp. 329–339, 2017.
- [96] S. Afifi, H. GholamHosseini, and R. Sinha, "A system on chip for melanoma detection using FPGA-based SVM classifier," *Microprocessors and Microsystems*, vol. 65, pp. 57–68, 2019.
- [97] A. K. Kushwaha and S. K. Paul, "Inductorless realization of Chua's oscillator using DVCCTA," *Analog Integrated Circuits and Signal Processing*, vol. 88, no. 1, pp. 137–150, 2016.
- [98] K. Rajagopal, A. Karthikeyan, D. Prakash, and H. Chameleon, "Fractional order FPGA implementation," *Complexity*, vol. 2017, Article ID 8979408, 2017.
- [99] H. R. Abdolmohammadi, A. J. M. Khalaf, S. Panahi et al., "A new 4D chaotic system with hidden attractor and its engineering applications: analog circuit design and field programmable gate array implementation," *Pramana*, vol. 90, p. 70, 2018.
- [100] A. Karthikeyan and K. Rajagopal, "FPGA implementation of fractional-order discrete memristor chaotic system and its commensurate and incommensurate synchronisations," *Pramana*, vol. 90, p. 14, 2018.